ASME Winter Annual Meeting, ASME Aerospace and Materials Divisions, Adaptive Structures And Material Systems Symposium, November 14-19, 1999, Nashville, TN, AD-Vol. 59, MD-Vol. 87, pp. 39-46.

MODELING OF THE ELECTRO-MECHANICAL (E/M) IMPEDANCE RESPONSE OF A DAMAGED COMPOSITE BEAM

Victor Giurgiutiu* and Craig A. Rogers‡
Department of Mechanical Engineering
University of South Carolina, Columbia, SC 29208
Phone: 803-777-8018, FAX: 803-777-0106, E-mail: *victorg@sc.edu*

ABSTRACT[1]

The electro-mechanical (E/M) impedance method has gained acceptance as an effective technique for structural health monitoring, damage detection, and failure prevention. In spite of extensive experimental validation of this novel method, very little work has been dedicated to its modeling. This paper develops a model of the E/M impedance response of a damaged composite beam interrogated by a PZT wafer active sensor. The electro-mechanical model for the interaction between the beam and the active sensor is developed from first principles. The effective axial force and bending moments induced by the PZT wafer into the beam are considered. Equations of motion for the flexural vibrations of a composite beam under moment excitation are developed. Solution in terms of normal modes with internal damping is obtained. The resulting response and the applied force are utilized to deduce general expressions for pointwise dynamic stiffness and pointwise dynamic compliance. Effective stiffness of the PZT wafer is also calculated, and the complex stiffness ratio for the PZT-structure interaction is determined. Hence, the complex electro-mechanical impedance and admittance are deduced.

A numerical example is given to illustrate the method and test its effectiveness. It is found that the real part of the effective pointwise dynamic stiffness interacts at par with the PZT stiffness at structural resonance frequencies. The imaginary part of the complex stiffness ratio directly reflects the pointwise structural resonances. Consequently, the real part of the electro-mechanical impedance directly reflects the pointwise structural resonances too. The same behavior is also found in the electro-mechanical admittance. Thus, the real part of the E/M impedance and the real part of the E/M admittance are found to be direct measures of the structural response, reflective of damage presence.

INTRODUCTION

Health monitoring of structures and machinery is a major concern of the engineering community. Flaws identification, early damage detection, and failure prevention are desiderates with far reaching implications in the management and preservation of nations aging infrastructure. Among structural health monitoring techniques, the electro-mechanical (E/M) impedance for structural health monitoring and non-destructive evaluation is an emerging method that offers distinct advantages. The electro-mechanical (E/M) impedance method has gained acceptance as an effective technique for structural health monitoring, damage detection, and failure prevention (Rogers and Giurgiutiu, 1999; Giurgiutiu and Rogers; 1999). The method uses small-size active sensors intimately bonded to an existing structure, or embedded into a new composite construction. Piezoelectric (PZT) wafer transducers have been widely used to this purpose. Experimental demonstrations have shown that the high-frequency impedance spectrum is directly affected by the presence of damage or defects in the monitored structure.

A precursor to the electromechanical impedance method is the mechanical impedance method. This method evolved in the late 1970's and early 1980's and was based on measuring the response to force excitation applied normal to structural surface using conventional shakers and velocity transducers. Cawley (1984) studied the mechanical impedance method for non-destructive inspection (NDI). He excited the vibrations of bonded plates using a specialized transducer that simultaneously measures the applied normal force and the induced velocity. In his study, Cawley (1984) extended the work of Lange (1978), and studied the behavior of bonded thin plates, in order to identify local disbonds. Finite element analysis of the vibration of the bonded/disbonded plates was performed, and the impedance to excitation in the normal direction was predicted. The experimental work measured the normal-direction impedance at various locations. A small shaker was used to apply excitation through a force gauge and an accelerometer connected to the structure. The

*Member, ASME
‡Fellow, ASME

impedance magnitude spectrum below the anti-resonance frequency was compared with the finite element predictions, and some correlation with the presence of disbonds was attempted. Phase information was not used in the data analysis. Since these early studies, the mechanical impedance method has evolved and gained its own place among NDE techniques. Currently, ultrasonic equipment manufacturers offer mechanical impedance analysis (MIA) probes and equipment as standard options (e.g., Staveley NDT Technologies, 1998). The mechanical impedance method is used to detect disbonds in laminated structures, and delaminations inside composite materials up to depth of 1/4-in.

The electro-mechanical impedance method takes the mechanical impedance concepts to the new horizons offered by the use of small-wafer piezoelectric active sensors intimately affixed to the structure. Force excitation normal to the structural surface is replaced by strain excitation in the plane of the surface. High frequency excitation in the high kHz low MHz region can be achieved. The bulky ultrasonic transducer of the mechanical impedance method (typically, 1" x 3-4") is replaced by a thin wafer active sensor. In addition, since the E/M impedance sensor is permanently attached to the surface (or embedded in composite structures), the force coupling issue associated with conventional ultrasonics is no longer a problem. The E/M impedance active sensors, hard wired into the structure, can be interconnected into sensor arrays. Through the intimate electro-mechanical coupling, the structural impedance is measured almost directly, whereas in the mechanical impedance method, post-processing of separately measured force and acceleration or velocity data was required.

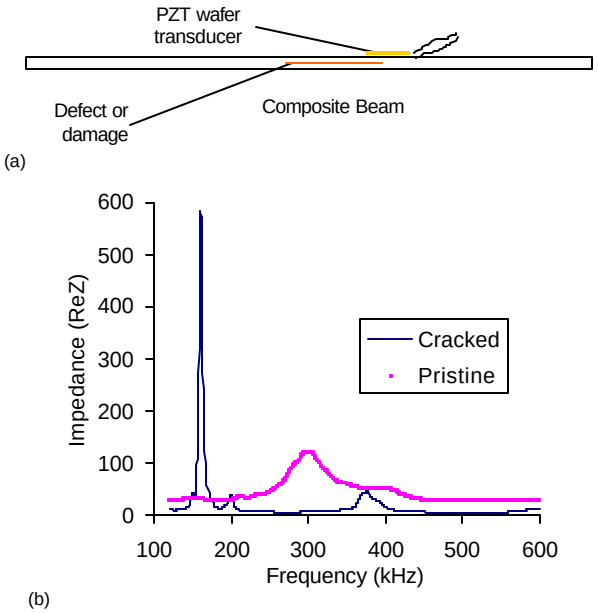

Figure 1 PZT wafer transducer acting as active sensor to monitor structural damage: (a) mounting of the PZT wafer transducer on a damaged structure; (b) the change in E/M impedance due to the presence of a crack.

Until now, the electro-mechanical impedance technique has evolved mainly through experimental discovery and proof-of-concept demonstrations. However, little theoretical work has been done so far to determine the analytical model that will permit to correctly predict the E/M impedance response for a given structure and its change with the progression of damage. Rossi *et al.* (1993) studied impedance modeling of piezoelectric actuator driven circular rings, but their analysis did not determine closed form solution. Their numerical examples were confined to relatively low frequencies (< 1.8 kHz). Liang *et al.* (1996) developed the impedance analysis of a PZT affixed to a structure, but did not detail a model for the structural response. Esteban (1996) attempted an analysis of beam vibrations with attached PZT wafers, but could not get fully conclusive results. The present paper will describe modeling efforts focused on determining the interaction between the PZT wafer transducer in terms of high-frequency vibration modes and point-wise structural impedance of pristine and damaged structure that directly affect the E/M impedance. The focus of this paper will be on the analysis of a damaged composite beam. Extension to plates and other composite structures is planned for future work.

ELECTRO-MECHANICAL IMPEDANCE

The electro-mechanical impedance method for structural health monitoring, damage detection, and NDE was explained in detail by Rogers and Giurgiutiu (1997) and by Giurgiutiu and Rogers (1997). A overview of its principles is given next. Consider a piezo-electric transducer wafer intimately bonded to the surface of a structural member. When excited by an alternating electric voltage, the piezo-electric transducer applies a local strain parallel to the surface. Thus, elastic waves are transmitted into the structure. The structure responds by presenting to the transducer the drive-point mechanical impedance $Z_{str}(w) = iwm_e(w) + c_e(w) - ik_e(w)/w$. Through the mechanical coupling between the PZT transducer and the host structure, and through the electro-mechanical transduction inside the PZT transducer, the drive-point structural impedance directly reflects into the effective electrical impedance as seen at the transducer terminals (Figure 1).

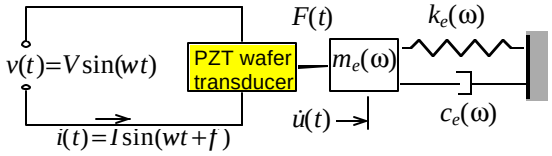

Figure 2 Electro-mechanical coupling between the PZT transducer and the structure.

The electro-mechanical (E/M) impedance technique for health monitoring, damage detection, and NDE (Rogers and Giurgiutiu, 1997) utilizes the changes that take place in the drive-point structural impedance to identify incipient damage in the structure.

The apparent electro-mechanical impedance of the piezo-transducer as coupled to the host structure is given by

$$Z(\omega) = \frac{1}{i\omega C}\left(1 - \kappa_{31}^2 \frac{k_{str}(\omega)}{k_{PZT} + k_{str}(\omega)}\right)^{-1}. \quad (1)$$

Here, $Z(w)$ is the electro-mechanical impedance as seen at the PZT transducer terminals, C is the zero-load capacitance of the PZT transducer, k_{31} is the electro-mechanical cross coupling coefficient of the PZT transducer ($\kappa_{31} = d_{13}/\sqrt{\bar{s}_{11}\bar{\varepsilon}_{33}}$), $k_{str}(\omega)$ is the dynamic stiffness of the structure, and k_{PZT} is the stiffness of the PZT-wafer active sensor. The electro-mechanical impedance method is applied by scanning a predetermined frequency range in the hundreds of kHz band and recording the complex impedance spectrum. By comparing the impedance spectra taken at various times during the service life of a structure, meaningful information can be extracted pertinent to structural degradation and the appearance of incipient damage (Figure 2b). It must be noted that the frequency range must be high enough for the signal wavelength to be significantly smaller than the defect size (Figure 2a).

The purpose of the present investigation is to determine analytical models for predicting the structural and PZT contributions to Equation (1). Such model will permit prediction of the E/M impedance, $Z(\omega)$, for a given structure, will allow determination of the method sensitivity to detect a certain defect size, and will permit the matching of sensor size and excitation level with structural type and defect size. Details of these developments beyond the limited space of this paper can be found in the full-length report by Giurgiutiu and Rogers (1999).

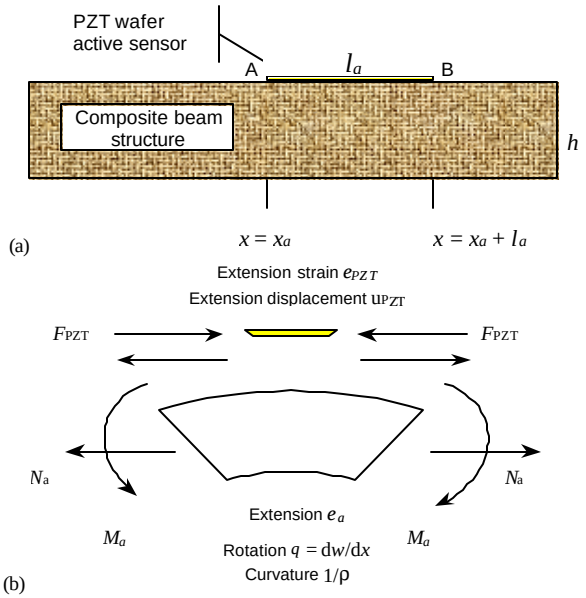

Figure 3 Model of the interaction between a PZT active sensor and a substrate beam structure: (a) geometry; (b) forces and moments.

MODEL DEFINITION

Consider a substrate beam with a PZT active sensor attached to it surface (Figure 3a). The active sensor has length l_a, and lies between x_a and $x_a + l_a$. Upon activation, the PZT active sensor expands by e_{PZT}. This generates a reaction force F_{PZT} from the beam structure. The reaction force is perceived by the beam structure as axial force, N_{PZT}, and bending moment, M_{PZT} at the neutral axis (Figure 3b).

As the active sensor is excited with a high-frequency harmonic signal, its expansion, ε_{PZT}, will follow a high-frequency sinusoidal oscillation. This oscillation induces elastic waves into the beam structure. The elastic waves travel sideways into the beam structure and set it up into oscillation. When the steady state regime is reached, the structure will exhibit sustained oscillations at the frequency of PZT excitation. The reaction force per unit displacement presented by the structure to the PZT will depend on the internal state of the structure, on the excitation frequency, and on the boundary conditions. For high frequency excitation, local modes of vibration are dominant, and the far-field boundary conditions become irrelevant.

The reaction force per unit displacement is expressed as:

$$k_{str}(\omega) = \hat{F}_{PZT}(\omega) / \hat{u}_{PZT}(\omega), \quad (2)$$

where $\hat{u}_{PZT}(\omega)$ is the displacement amplitude at frequency ω, $\hat{F}_{PZT}(\omega)$ is the reaction force, and $k_{str}(\omega)$ is the dynamic stiffness. The symbol ^ signifies amplitude. Since the size of the PZT is very small with respect to the size of the structure, formula (2) represents a point-wise structural stiffness. Upon division by ω, one can also get the point-wise structural impedance:

$$Z_{str}(\omega) = k_{str}(\omega)/\omega. \quad (3)$$

MODELING OF THE STRUCTURAL SUBSTRATE

The response of the structural substrate to the PZT excitation is deduced following the general theory of beam vibrations (Timoshenko, 1955; Inman, 1996.) However, Excitation is through a pair of axial forces and bending moments separated by a small but finite distance, l_{PZT}. This feature departs the present analysis from a typical textbook formulation.

Definition of the Excitation Forces and Moments

The excitation forces and moments acting upon the beam structure are derived from the PZT force using the beam cross-section geometry (Figure 3):

$$M_a = F_{PZT}\frac{h}{2}, \quad N_a = F_{PZT} \quad (4)$$

The space-wise distribution of excitation bending moment and axial force are expressed using the Heaviside function,

$$H(x - x_a) = \begin{cases} 0, & x < x_a \\ 1, & x \geq x_a \end{cases}. \quad (5)$$

Hence, the actuation force and moment are:

$$N_e(x,t) = N_a\left[H\left(x - x_a\right) - H\left(x - x_a - l_a\right)\right]\cdot e^{iwt} \qquad (6)$$

$$N_e(x,t) = M_a\left[H\left(x - x_a\right) - H\left(x - x_a - l_a\right)\right]\cdot e^{iwt} \qquad (7)$$

Equations (6) and (7) correspond to axial and flexural vibrations, respectively.

Axial Vibrations

Axial vibrations modes are usually of much larger frequency than flexural vibration modes. They will not be considered in the present analysis.

Flexural Vibrations

Since the flexural excitation, Equation (7), is in the form of a moment, the equation of motions for flexural vibrations have to be described in terms of *curvature waves*. Consider an infinitesimal beam element of length d*x*, placed between *x* and *x* + d*x*, under the action of an external distributed bending moment *m*(*x*, *t*) as shown in Figure 4. The units of *m*(*x*, *t*) are [Nm/m]

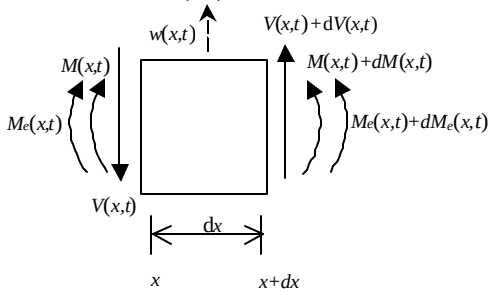

Figure 4 Free-body diagram of a beam element subjected to distributed bending moment excitation.

Consider an infinitesimal beam element of length d*x*, placed between *x* and *x* + d*x*, under the action of an external bending moment $M_e(x, t)$, as shown in Figure 4. Ignoring rotary inertia, write:

$$r A\cdot \ddot{w}\cdot \mathrm{d}\,x = \mathrm{d}\,V \qquad (8)$$

$$\mathrm{d}\,M + \mathrm{d}\,M_e + V\,\mathrm{d}\,x = 0 \qquad (9)$$

Euler- Bernoulli's theory of bending gives

$$M = EI\cdot w'' . \qquad (10)$$

Substituting Equation (10) into Equation (9) yields

$$EI\cdot w''' + M_e' + V = 0 . \qquad (11)$$

Substitution of Equation (11) into Equation (8) gives, upon rearrangement,

$$r A\cdot \ddot{w}(x,t) + EI\cdot w''''(x,t) = -M_e''(x,t) \qquad (12)$$

Assume solution in the form:

$$w(x,t) = \sum_{n=N_1}^{N_2} T_n(t)X_n(x) \qquad (13)$$

where $T_n(t)$ is the time-varying modal response, and N_1 and N_2 are the power and upper mode numbers bracketing the high-frequency interval under investigation. Also, assume steady-state response at the excitation frequency, *w*, i.e.

$$w(x,t) = \sum_{n=N_1}^{N_2} C_n X_n(x)\cdot e^{iwt} \qquad (14)$$

Substitution into the differential equation and cancellation of the time-varying harmonic function on both sides of the equation yields the space-wise differential equation:

$$-w^2 r A\cdot\sum_n C_n X_n(x) + EI\cdot\sum_n C_n X_n''''(x) = -\hat{M}_e''(x) \qquad (15)$$

Invoke the differential equation defining the natural modes of flexural vibration:

$$EI\cdot X_n'''' = w_n^2\cdot r A\cdot X_n \qquad (16)$$

Hence, Equation (15) becomes

$$r A\cdot\sum_n \left(w_n^2 - w^2\right)C_n X_n(x) = -\hat{M}_e''(x) \qquad (17)$$

Following the Galerkin approach, multiply by $X_m(x)$ and integrate over the length of the beam:

$$r A\sum_n C_n\left(w_n^2 - w^2\right)\int_0^l X_m(x)X_n(x)\,\mathrm{d}\,x = -\int_0^l X_m(x)\hat{M}_e''(x)\,\mathrm{d}\,x \qquad (18)$$

Invoke modeshapes ortho-normality:

$$\int_0^l X_m(x)X_n(x)\,\mathrm{d}\,x = d_{mn} = \begin{cases}1, & m = n\\ 0, & m \neq n\end{cases} . \qquad (19)$$

define the modal excitation as:

$$X_{0n} = -\frac{1}{r A}\int_0^l X_n(x)\hat{M}_e''(x)\,\mathrm{d}\,x , \qquad (20)$$

and assume viscous damping, *z*.. Hence, the general solution:

$$C_n = \frac{X_{0n}}{\left(w_n^2 + 2izww_n - w^2\right)} \qquad (21)$$

Explicit calculation of X_{0n} yields:

$$X_{0n} = -\frac{M_a}{r A}\int_0^l X_n(x)\left[d'\left(x - x_a\right) - d'\left(x - x_a - l_a\right)\right]\mathrm{d}\,x \qquad (22)$$

Upon integration by parts,

$$X_{0n} = -\frac{M_a}{r A}\left[X_n'\left(x - x_a\right) - X_n'\left(x - x_a - l_a\right)\right] \qquad (23)$$

To obtain the structural dynamic stiffness seen by the PZT wafer, calculate the displacements at points A & B,

$$u_A = -\frac{h}{2}w'(x_a,t), \quad u_B = -\frac{h}{2}w'(x_a + l_a,t) \qquad (24)$$

and find the elongation of the PZT wafer:

$$u_{PZT}(t) = u_B(t) - u_A(t) = \frac{h}{2}\sum_n\left[X_n'(x_a) - X_n'(x_a + l_a)\right]C_n e^{iwt} \qquad (25)$$

Substitution of C_n and X_{0n} yields:

$$\hat{u}_{PZT} = F_{PZT} \frac{\left(\frac{h}{2}\right)^2}{r\,A} \sum_n \frac{\left[X_n'(x_a) - X_n'(x_a + l_a)\right]^2}{w_n^2 + 2izww_n - w^2} \tag{26}$$

Hence,

$$k_{str} = \frac{F_{PZT}}{\hat{u}_{PZT}} = \left\{ \frac{\left(\frac{h}{2}\right)^2}{r\,A} \sum_n \frac{\left[X_n'(x_a) - X_n'(x_a + l_a)\right]^2}{w_n^2 + 2izww_n - w^2} \right\}^{-1} \tag{27}$$

For pinned-pinned beams, the mode shapes are (Inman, 1996):

$$X_n(x) = A_n \sin(b_n x), \quad A_n = \sqrt{2/l}, \quad b = \left(w^2 r A / EI\right)^{1/4} \tag{28}$$

Upon substitution,

$$k_{str}(w) = \left\{ \frac{h^2}{r\,A} \sum_n \frac{\left[A_n b_n(w) \sin\left(b_n(w)\frac{2x_a + l_a}{2}\right) \sin\left(b_n(w)\frac{l_a}{2}\right)\right]^2}{w_n^2 + 2izww_n - w^2} \right\}^{-1} \tag{29}$$

MODELING OF THE PZT ACTIVE SENSOR

Consider a PZT wafer of length lPZT, thickness t, and width b (Figure 5). The 3-D constitutive equations of the PZT material are, in Physics notations,

$$\begin{aligned} S_{ij} &= s_{ijkl}^E T_{kl} + d_{kij} E_k \\ D_j &= d_{jkl} T_{kl} + \varepsilon_{jk}^T E_k \end{aligned} \tag{30}$$

where S_{ij} is the mechanical strain, T_{ij} is the mechanical stress, E_i is the electrical field, D_i is the electrical displacement, s_{ijkl}^E is the mechanical compliance at zero electric field (E = 0), ε_{jk}^T is the dielectric constant (impermittivity) at zero mechanical stress (T = 0), and d_{kij} is the piezoelectric coupling between the electrical and mechanical variables. Attention is focused on the longitudinal expansion, u_1, induced by the thickness polarization, E_3. Thus, Equation (28) becomes:

$$\begin{aligned} S_1 &= s_{11}^E T_1 + d_{31} E_3 \\ D_3 &= d_{31} T_1 + \varepsilon_3^T E_3 \end{aligned} \tag{31}$$

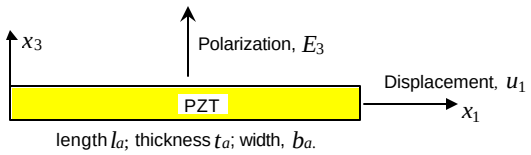

Figure 5 Schematic representation of a PZT wafer active sensor.

The mechanical stiffness of the PZT active sensor with respect to an axial force applied in the x_1 direction is

$$k_{PZT} = \frac{A_a}{s_{11} l_a}, \tag{32}$$

where $A_a = t_a \cdot b_a$ is the PZT cross-sectional area. Because of the its small dimensions, longitudinal wave propagation effects in the PZT wafer are negligible, and Equation (30) can be used for both static and dynamic regime. In other words, the strain induced in the PZT wafer is unaffected by dynamic effects and hence uniform along the PZT length.

NUMERICAL EXAMPLE

For exemplification, consider a uniform beam of l = 100 mm, h = 3 mm, and b = 19.6 mm, made of carbon fiber epoxy composite with E_{11} = 200 GPa and ρ = 1600 kg/m^3. A PZT wafer active sensor is affixed to the top surface of the beam at x_a = 40 mm. The PZT-wafer active-sensor dimensions are l_a = 4.5 mm, b_a = 4.5 mm, t_a = 0.200 mm. The properties of the PZT material are given in Table 1.

Table 1 Properties of the active-sensor PZT material

Name	Symbol	Value
Compliance	s_{11}	$15.2 \cdot 10^{-12}$ Pa^{-1}
Dielectric constant	ε_{33}	$7.427 \cdot 10^{9}$ F/m
Induced strain coefficient	d_{13}	$-125 \cdot 10^{-12}$ m/V

Natural Frequencies

The frequency range 100 kHz to 400 kHz was scanned for natural frequencies of the beam. this investigation revealed that 9 modes bracket this interval, such that the lower mode corresponds to N_1 = 8, and the upper mode to N_2 = 17. Table 2 gives the values of the mode numbers and the corresponding frequencies. Notice that of the 9 modes, only 7 (modes 9 through 16, underlined) lie strictly between 100 kHz and 400 kHz.

Table 2 Frequencies considered for analysis in the 100 kHz to 400 kHz frequency range

Mode #	8	9	10	11	12	13	14	15	16	17
Frequency, kHz	97	123	152	184	219	257	298	342	389	440

Vibration Response

Figure 6 shows the response of the beam (dynamic compliance) for high-frequency active-sensor excitation in the range 100÷400 kHz. The response is measured with respect to the PZT excitation force applied to the surface of the beam in a pinching action, and is drawn for an excitation force of unit value.

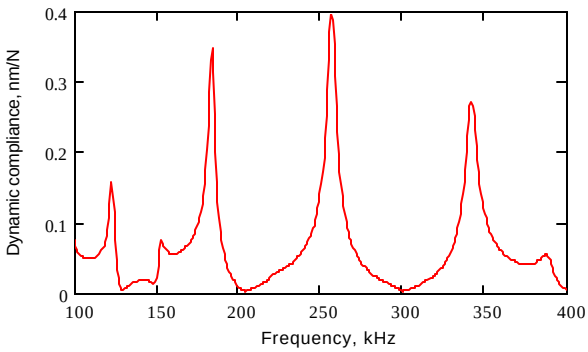

Figure 6 Response of a composite beam to unit force excitation (dynamic compliance) from a PZT wafer active sensor in the frequency range 100 to 400 kHz.

The plot in Figure 6 reveals that not all of the 7 modes present in the frequency range of interest are equally excited. This aspect is consistent with the fact that various modes have different mode shapes that may or may not happen to have significant curvature at the point where the PZT wafer active sensor is affixed. In our case, modes 9 (123 kHz), 11 (183 kHz), 13 (257 kHz), and 15 (342 kHz) are very active, mode 8 (97 kHz) is marginally active, while modes 10 (152 kHz), 12 (219 kHz) and 16 (389 kHz) are dormant and difficult to identify.

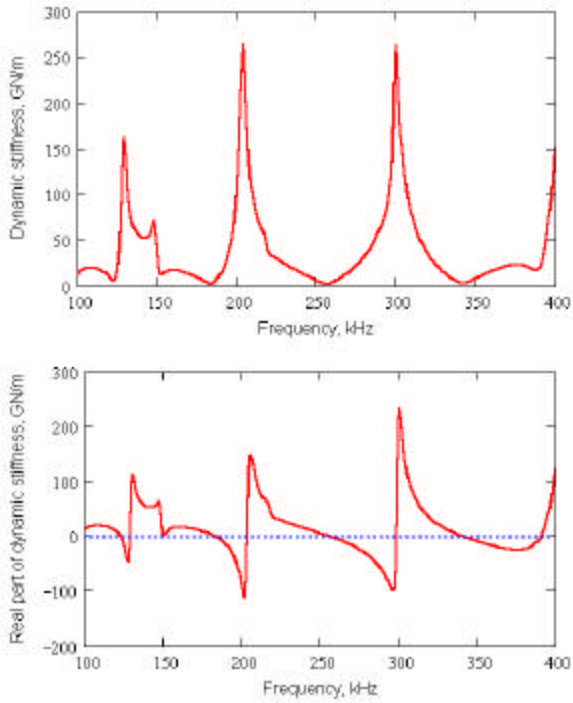

Figure 7 Dynamic stiffness and presented by the composite beam to the PZT wafer active sensor in the frequency range 100- 400 kHz.

Pointwise Structural Stiffness

The pointwise dynamic structural stiffness, $k_{str}(\omega)$, with respect to surface excitation of the beam by PZT is given in Figure 7. Please note that, since the dynamic stiffness is the inverse of the response to unit excitation, the peaks and valleys from one diagram correspond to valleys and peaks in the other. Thus, at points where the dynamic response has a maximum, the dynamic stiffness has a minimum, and vice-versa.

Also plotted in Figure 7 is the mechanical stiffness of the PZT, k_{PZT} = 0.013 GN/m. The PZT stiffness, k_{PZT}, is superposed on the plot of the real part of the structural impedance, Re(k_{str}). It should be appreciated that the real part of the structural impedance goes through zero at the structural resonance frequencies. Hence, near structural resonance frequencies, the PZT stiffness and the real part of the structural stiffness become comparable. This observation is crucial for understanding the mechanism of electro-mechanical coupling between the active sensor and the structural substrate.

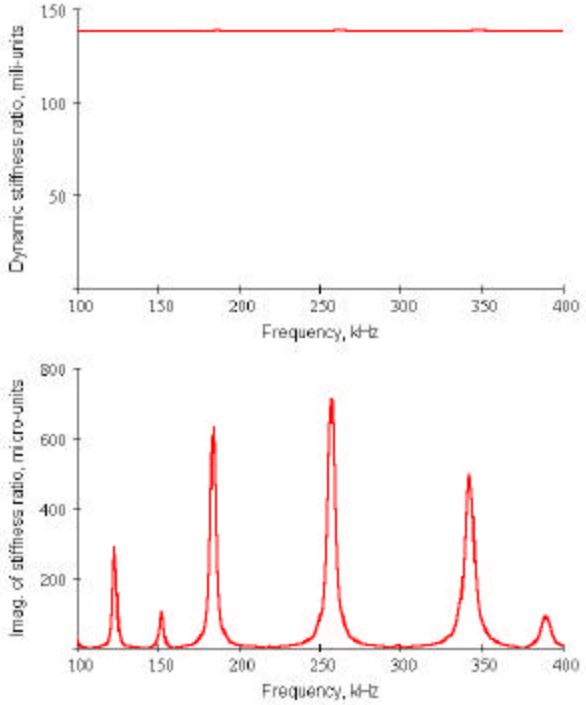

Figure 8 Dynamic stiffness ratio fora composite beam and a PZT wafer active sensor in the frequency range 100-400 kHz.

Dynamic Stiffness Ratio

Figure 8 presents the dynamic stiffness ratio between the structure and structure plus PZT, as used in Equation (1), i.e.,

$$r(\omega) = \frac{k_{str}(\omega)}{k_{PZT} + k_{str}(\omega)} \qquad (33)$$

Note that the magnitude is almost constant around the $139 \cdot 10^{-3}$ value. However, the imaginary part of the dynamic stiffness ratio, though much smaller in value, displays a peaks and valleys pattern that follow closely the structural-response resonance pattern displayed in the dynamic compliance plot of Figure 6. This observation is essential to understanding how the electro-mechanical (E/M) impedance method is able to detect the dynamic behavior of the structure.

Further more, the spectrum presented by the imaginary part of the dynamic stiffness ratio (Figure 8) has a better frequency resolution that the mechanical response. Recall that inspection of the dynamic response (Figure 6) identified 4 active modes, i.e., modes 9 (123 kHz), 11 (183 kHz), 13 (257 kHz), and 15 (342 kHz); one marginally active, mode 8 (97 kHz); and 3 dormant modes 10 (152 kHz), 12 (219 kHz) and 16 (389 kHz). Inspection of the dynamic stiffness ratio identifies the same 4 active modes (#9, 11, 13, and 15), but also clearly identifies the marginally active mode 8 (150 kHz) and 2 of the dormant modes (#8 @ 87 kHz, and #16 @ 389 kHz). The only mode not identified is #12 @ 219 kHz.

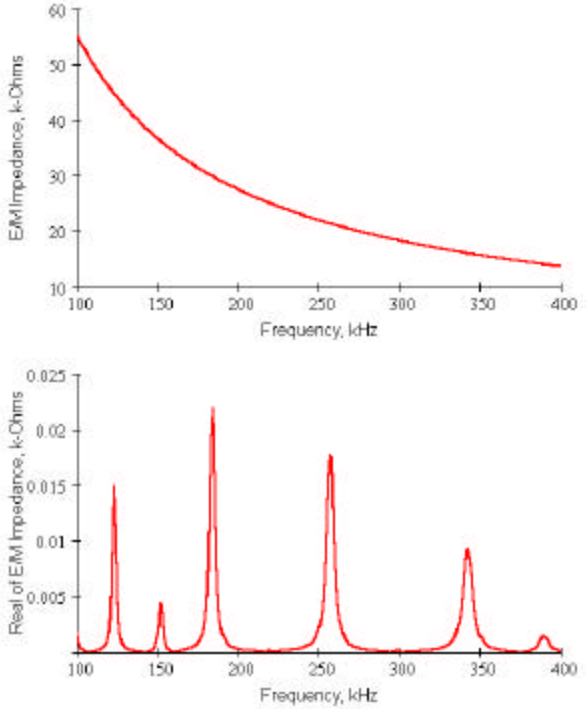

Figure 9 High frequency E/M impedance and its real part for a small PZT-wafer active sensor affixed to the surface of a composite beam

Electro-Mechanical (E/M) Impedance

Figure 9 shown the real and imaginary components of the electro-mechanical (E/M) impedance as would have been measured at the electrical terminals of the PZT-wafer active sensor. In these graphs, the E/M impedance magnitude is dominated by the $1/i\omega C$ component. Hence, it does not display any noticeable variations as resonance frequencies are passed through. Whereas the real part of the E/M impedance, though generally much smaller in value, follows closely the structural-response resonance pattern displayed in the dynamic compliance plot of Figure 6.

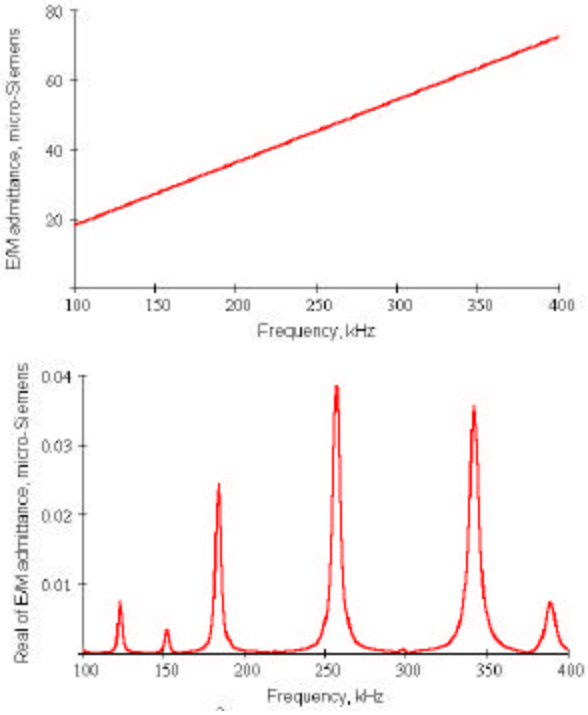

Figure 10 High frequency E/M admittance and its real part for a small PZT-wafer active sensor affixed to the surface of a composite beam

Electro-Mechanical (E/M) Admittance

Figure 10 gives the real and imaginary components of the E/M admittance as would have been measured at the electrical terminals of the PZT-wafer active sensor. The E/M admittance is the inverse of the E/M impedance and is given by:

$$Y(\omega) = i\omega C\left(1 - \kappa_{31}^2 \frac{k_{str}(\omega)}{k_{PZT}(\omega) + k_{str}(\omega)}\right). \qquad (1)$$

In the graphs of Figure 10, the E/M admittance magnitude is dominated by the $i\omega C$ component. Hence, it does not display any noticeable variations as resonance frequencies are passed through. Whereas the real part of the E/M admittance, though generally much smaller in value, follows closely the structural-response

resonance pattern displayed in the dynamic compliance plot of Figure 6.

Comparison of Mechanical Response, E/M Impedance Signature, and E/M Admittance Signature

The preceding graphs have indicated that the structural dynamic response pattern (prominent peaks at resonance frequencies) is recovered in the pointwise dynamic stiffness, in the real part of the E/M impedance, and in the real part of the E/M admittance.

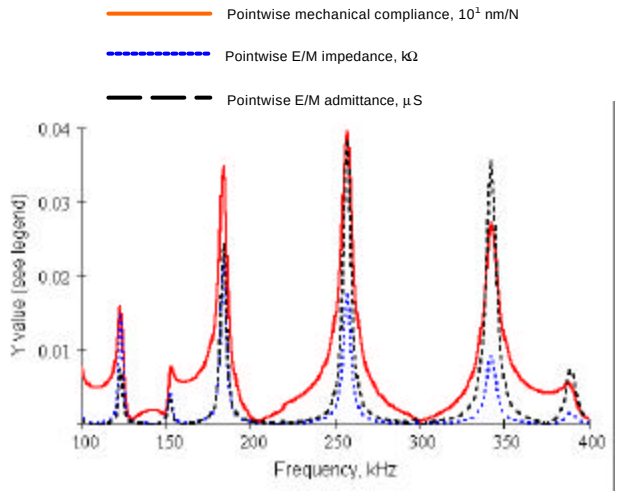

Figure 11 Pointwise mechanical compliance, E/M impedance, and E/M admittance of a composite beam

Figure 11 displays these three variables superposed on the same graph for easy comparison. It can be seen that all three concepts (mechanical compliance, E/M impedance, and E/M admittance) identify equally well the structural resonance frequencies. Their behavior around resonance frequencies is similar, but not identical. The E/M impedance has a stronger response towards lower frequencies, while the E/M admittance has a stronger response towards higher frequencies.

Effect of Structural Damage

Figure 12 shows how the E/M impedance signature changes when damage takes place in the beam. In this example, damage was simulated by varying the thickness of the beam. This thickness change corresponds to a delamination, which virtually splits the beam into two regions, such that the PZT wafer active sensor remains attached to a locally thinner beam. In our simulation, a 55% effective post-lamination thickness was considered. The clear difference between the two signatures, pristine and damaged, is apparent. The plots in Figure 12 indicate that the effect of damage is to shift to the left the resonance frequency peaks, and to increase their value. These modifications in the E/M impedance signature are essential in identifying the presence of structural damage.

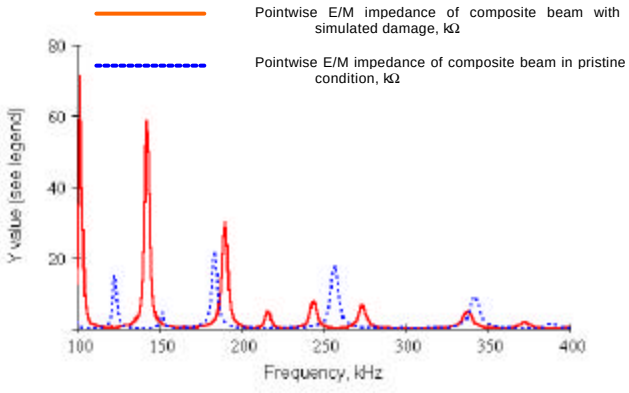

Figure 12 Pointwise mechanical compliance, E/M impedance, and E/M admittance of a composite beam with simulated damage (45% effective thickness decrease due to delamination).

CONCLUSIONS

The electro-mechanical (E/M) impedance method has gained acceptance as an effective technique for structural health monitoring, damage detection, and failure prevention. In spite of extensive experimental validation and proof-of-concept demonstrations, little work has been dedicated to its modeling. This paper presented a model for the E/M impedance response of a damaged composite beam interrogated by a PZT wafer active sensor developed from first principles. The effective axial force and bending moments induced by the PZT wafer into the beam were considered. Equations of motion for composite beam flexural vibrations under moment excitation were developed. Solution in terms of normal modes with internal damping was obtained. The resulting response and the applied force were utilized to deduce general expressions for pointwise dynamic stiffness and pointwise dynamic compliance to in-plane surface excitation. Effective stiffness of the PZT wafer was calculated, and the complex stiffness ratio for the PZT-structure interaction was determined. Hence, the complex electro-mechanical impedance and admittance were deduced.

A numerical example was given to illustrate the method and test its effectiveness. It was found that the real part of the effective pointwise dynamic stiffness interacts at par with the PZT stiffness at structural resonance frequencies. Pointwise structural resonances were found to be directly reflected in the imaginary part of the complex stiffness ratio, and in the real part of the electro-mechanical impedance. The same behavior was also found in the electro-mechanical admittance. Thus, the real part of the E/M impedance and the real part of the E/M admittance were identified as direct measures of the structural response. When simulated damage was introduced, shifts in the response peaks and modification of peak amplitudes, obtained in the mechanical response, were traced directly into the similar shifts in the E/M impedance and admittance real parts.

ACKNOWLEDGMENTS

The authors gratefully acknowledge the financial support of the National Science Foundation through NSF/EPSCoR Cooperative Agreement No. EPS-9630167 and of the US Department of Defense through South Carolina Army National Guard.

REFERENCES

CAWLEY, P. (1984) "The Impedance Method for Non-Destructive Inspection", *NDT International*, Vol. 17, No. 2, 1984, pp. 59-65.

CRAWLEY, Edward F.; ANDERSON, Eric H. (1990) "Detailed Models of Piezoceramic Actuation of Beams", *Journal of Intelligent Material Systems and Structures*, Vol.1, No. 1, 1990, pp. 5-25.

CRAWLEY, Edward F.; de LUIS, Javier (1987) "Use of Piezoelectric Actuators as Elements of Intelligent Structures", *AIAA Journal*, Vol. 25, No. 10, pp. 1373-1385, 1987.

ESTEBAN, J.; LALANDE, F.; ROGERS, C. A. (1996) "Parametric Study on the Sensing Region of a Collocated PZT Actuator-Sensor," *Proceedings, 1996 SEM VIII International Congress on Experimental Mechanics*, 10-13 June, 1996.

GIURGIUTIU, V.; CHAUDHRY, Z.; ROGERS C. A. (1994) "The Analysis of Power Delivery Capability of Induced Strain Actuators for Dynamic Applications," *2nd International Conference on Intelligent Materials*, Williamsburg, VA, 5-8 June 1994, pp. 565-576.

GIURGIUTIU, V.; ROGERS, C. A. (1997) "The electro-mechanical (E/M) impedance method for structural health monitoring and non-destructive evaluation", *International Workshop on Structural Health Monitoring*, Stanford University, CA, September 18-20, 1997.

GIURGIUTIU, V.; ROGERS, C. A. (1998) "Recent Advancements in the Electro-Mechanical (E/M) Impedance Method for Structural Health Monitoring and NDE, *Proceedings of the SPIE's 5th International Symposium on Smart Structures and Materials*, 1-5 March 1998, Catamaran Resort Hotel, San Diego, CA, pp. 536-547.

GIURGIUTIU, V.; ROGERS, C. A. (1999) "Modeling of the electro-mechanical (E/M) impedance method applied to a composite beam", Report # USC-ME-LAMSS-99-105, May 29, 1999.

INMAN, J. D. (1996) *Engineering Vibration*, Prentice Hall, 1996.

LANGE, Yu. V. (1984) "Characteristics of the Impedance Method of Inspection and of Impedance Inspection Transducers", *Soviet Journal of Nondestructive Testing*, 1978, pp. 958-966.

LIANG, C.; SUN, F. P.; ROGERS C. A. (1996) "Electro-mechanical Impedance Modeling of Active Material Systems," *Smart Materials and Structures*, Vol. 5, pp. 171-186.

LIN, M. W.; ROGERS, C. A. (1993) "Modeling of the Actuation Mechanism in a Beam Structure with Induced Strain Actuators", paper # AIAA-93-1715-CP, 1993, pp. 3608-3617.

LIN, M. W.; ROGERS, C. A. (1994) "Bonding Layer Effects on the Actuation Mechanism of an Induced Strain Actuator/Substructure System", *SPIE Vol. 2190*, 1994, pp. 658-670.

ROGERS, C. A.; GIURGIUTIU, V. (1997) "Electro-Mechanical (E/M) Impedance Technique for Structural Health Monitoring and Non-Destructive Evaluation", Invention Disclosure No. 97162, University of South Carolina Office of Technology Transfer, July 1997.

ROGERS, Craig A. (1993) "Structural Impedance Modification and Energy Consideration for Structural Control", *Technical Memorandum of PWRI No. 3217, ISSN 0386-5878*, May 1993, pp. 355-380.

TIMOSHENKO, S. (1955) *Vibration Problems in Engineering*, D. Van Nostrad Company, Inc., 1955.

WANG, Bor-Tsuen; ROGERS, Craig A. (1991) "Modeling of Finite-Length Spatially-Distributed Induced Strain Actuators for Laminate Beams and Plates", paper # AIAA-91-1258-CP, 1991, pp. 1511-1520.